UNIVERSITY OF CALIFORNIA, SAN DIEGO

A Performance Assessment of the WaveWatch III Ocean Wave Model in the Pacific Basin

A Thesis submitted in partial satisfaction of the requirements for the degree Master of Science

in

Oceanography

by

Lynne Hoppe

Committee in charge:

Eric Terrill, Co-Chair
William Hodgkiss, Co-Chair
Falk Feddersen
Sophia Merrifield

2018

The Thesis of Lynne Hoppe is approved, and it is acceptable in quality and form for publication on microfilm and electronically:

_____

_____

_____

Co-Chair

_____

Co-Chair

University of California, San Diego

2018

DEDICATION

Thank you to Eric Terrill for allowing me to be a part of this study and for creating an atmosphere that would be flexible enough for me to finish this thesis.

Thank you to Sophia Merrifield who is as brilliant as she is energetic. I'm amazed at the amount of work you're able to keep up with. Thank you for putting up with me throughout this thesis and taking far more time inching me through this process than should be needed for any one person.

Finally, thank you to my family. Addy and Dash, you had a few not fun weekends while I pushed through finishing. Thank you for your patience with me. Rob, you supported me and kept encouraging me throughout the process. And Dad, my biggest fan no matter what. You inspire me with your drive to get better at all things and to continue to stay knowledgeable in math and science. I would not be where I am without you!

TABLE OF CONTENTS

LIST OF FIGURES

LIST OF TABLES

ABSTRACT OF THE THESIS

A Performance Assessment of the WaveWatch III Ocean Wave Model in the Pacific Basin

by

Lynne Hoppe

Master of Science in Oceanography

University of California, San Diego, 2018

Eric Terrill, Co-Chair

William Hodgkiss, Co-Chair

A performance assessment of the WaveWatch III (WW3) Ocean Wave Model in the Pacific Basin is conducted by comparing spectral model output to observational data from 13 drifting, GPS-based wave buoys in the mid-latitudes of the Northern Pacific. The observational array captured significant wave heights exceeding 12m and wave conditions associated with extratropical cyclones generated off the coast of Japan. While most model comparison studies use data from buoys moored near coastlines, the drifting array used in this work provides a unique opportunity to study cross basin storm and swell propagation. Although there is good agreement between the bulk parameters measured by the buoys and modelled in WW3, discrepancies in the timing of storm propagation lead to model-data inconsistencies. Arrival biases up to 10 hours and significant wave height

discrepancies of 4m are documented. Additionally, at high-frequencies, the wave energy density modelled in WW3 is higher than the buoy measurements. Model-data biases in this study are postulated to be associated with errors in the wind-forcing field.

I. INTRODUCTION

Ocean wave models provide important forecast information for coastal communities during extreme events. In the open-ocean, accurate forecasts are crucial for the safe operation of vessels. In the U.S. Navy, ships and aircraft operate at sea for months on end. Timely and accurate prediction of winds and sea states are critical for meeting the tasked mission and keeping sailors safe. To maintain safety and maintenance of the ship, seas greater than 3.66m (12 feet) are avoided. For ships operating in the Northern Pacific, this limit poses significant navigational challenges. The potential for high winds and seas combined with the large fetch of the Pacific means ships must either travel greater distances to avoid rough weather or have accurate prediction models to minimize the chance they encounter it. Cargo ships also rely on accurate reporting of sea state and winds for safe passage and to minimize the amount of time in transit to maintain profitability. Cargo ships are often designed to encounter smaller than 11m waves (Smith 2007). Continued structural stress encountering large waves and high winds reduce the longevity of the container ships and reduce profits of the companies who own them.

Ocean wave models have been developed to represent the conditions of the ocean in time and space. Now in their third-generation, models continue to improve ocean wave physics parameterizations and take advantage of additional computing power not economical to previous generations of wave models (Tolman 2002). Wave models solve the spectral action balance equation:

$$\frac{\partial \mathrm{N(i)}}{\partial \mathrm{t}} + \nabla_{\mathrm{x}} \cdot (\mathrm{c_g} + \mathrm{U})\mathrm{N(i)} + \nabla_{\mathrm{i}} \cdot \mathrm{c_i N(i)} = \Sigma \mathrm{S(i)} \qquad \text{(Equation 1)}$$

where $N(i)$ is the action density, i is the spectral phase space (wavenumber, frequency, direction, 2D), ∇_x and ∇_i are divergence operators, c_g, U, and c_i are characteristic and current velocities, and $\Sigma S(i)$ are the sources and sinks of energy/action (Tolman 2002). In deep water, the net source term, S, is a balance between an atmosphere-wave interaction term S_{in}, which is usually a positive energy input but can also be negative in the case of swell; a nonlinear wave-wave interactions term S_{nl}; and a wave-ocean interaction term that represents the dissipation S_{ds} of wave energy as wave breaking. As models continue to improve their representation of the ocean, long duration, in-situ datasets are needed for validation studies, especially away from coastlines where moored measurements are difficult to obtain.

a. Previous wave model/observation comparison studies

A number of previous studies have validated wave models with observational data. In August 2001, the U.S. Navy transitioned from using the Wave Modeling (WAM) model to the WW3 model. Wingeart (2001) compared global wave forecast models output by two national forecast centers (Fleet Numerical Meteorology and Oceanography Center (FNMOC) and National Centers for Environmental Prediction (NCEP)), operating WAM and WWIII respectively. The former forced the model using Navy Operational Global Atmospheric Prediction System (NOGAPS) winds, and the latter used wind fields from the Global Data Assimilation System/ NCEP Global Aviation Model (GDAS/AVN). Using available deep-water (greater than 500m) buoy observations at a very limited number of locations, wave energy fluxes and swell propagation times were assessed. The study concluded that the WW3 model operated at NCEP was more accurate (specifically in the

Pacific area of the study) due to the wind fields that were driving the model, which accounted for the large Pacific storms that generate low-frequency swell. Additionally, the models tended to under-predict the total energy for swell events. Since this study, WW3 has gone through multiple upgrades in the numerics of the physics engines, and can be forced by a variety of wind models such as Global Forecast System (GFS) and Navy Global Environmental Model (NAVGEM) winds.

Bidlot et al. (2002) compared the performance of operational wave forecasting systems with moored buoy data catalogued from World Meteorological Organization (WMO)[1]. The European Centre for Medium-Range Weather Forecasts (ECMWF) model, the Met Office, the FNMOC model and the Atmospheric Environment Service (AES) model of Canada were compared to moored buoy data. These data were from the 40 buoys off the eastern North Atlantic, the west coast of Hawaii, off the Southern coast of Japan, and the East and West coast of the United States and Canada. The study found that the model under predicted significant wave heights relative to buoy measurements, which was attributed to the wind forcing. Additionally, the authors found that the lowest wave height errors were associated with the most accurate wind forcing field and that the models struggled at representing conditions on the western side of ocean basins (Japan, US east coast).

Rogers et al. (2005) compared different wind model forcings of WaveWatch III to determine if the wind field inputs were the sole source of the error seen in the forecast, or if there were specific errors in the wave model physics. When comparing WW3 with

[1] Locations of all buoys used in the comparison include Hawaii (HW), Japan (JAPAN), the North Pacific (NPC), U.S. west coast (USWC), U.S. east coast (USEC), Gulf of Mexico (GM), Canadian east coast (CANEC), the northeast Atlantic (NEATL), and the North Sea (NSEA) with data provided by the Japanese Meteorological Agency (JMA), the U.S. National Data Buoy Center (NDBC), the Canadian Marine Environmental Data Service (CMEDS), and the Met Office (UKMO).

NOGAPS and WW3 with NCEP forced winds, the models both biased low for significant wave height. When the models were adjusted with scatterometer-based wind fields, they both improved. Differences in the northern Pacific (compared to the Atlantic) were noted, where, due to the large fetch, swell driven energy dominates. The model tended to under predict energy at low frequencies and over predict energy at high frequencies.

b. WaveWatch III

The WW3 model was created in the 1990's by Hendrick Tolman (Tolman 1996) and can be forced by a variety of wind products. WW3 is currently the operational open ocean wave model choice of the both the U.S. Navy and the National Weather Service/National Oceanographic and Atmospheric Administration (NWS/NOAA). For the U.S. Navy, the model is run at FNMOC and provides new forecasts every six hours for most parameters out to a 180-hour period. Navy forecasters compare the WW3 model to other open ocean or coastal models as well as observations from ships, aircraft, and satellites to provide the most accurate forecast for deployed units. For this study, WW3 model hindcast data was provided by Erick Rogers (Stennis-NRL) and spectral output was saved at the location of the buoys as they drifted in time. The output had a spatial resolution of 0.5^{o}x0.5^{o} and temporal resolution of 3hr, corresponding to the report rate of the wave buoys. The model is forced with 0.28^{o} NAVGEM winds and includes the ST4 physics package (Ardhuin et al. 2010). To compare the buoys to WW3, the nearest neighbor grid location in WW3 is used. The latest version of the WW3 code, version 5, is current as of 2016 and is used in this study. As the model development team is

continually updating and refining their algorithms, this information is only current as of the 2016 updates.

c. Pacific Ocean circulation, storm formation, and seasonal variability

The location of the wave buoys during this study is between 24º- 39ºN and 158ºE-130ºW. In this region of the Northern Pacific Ocean, the overall geostrophic flow is from West to East. The buoys extend from the edge of the Kuroshio Extension and flow along the North Pacific Current (Talley et al. 2011, Figure 1) with a drift consistent with geostrophy. The North Pacific Current travels at speeds of 0.15-0.36 m/s in this region (McNally et al 1983). As predicted by the climatology of the region, the buoys flowed West to East along the North Pacific Current.

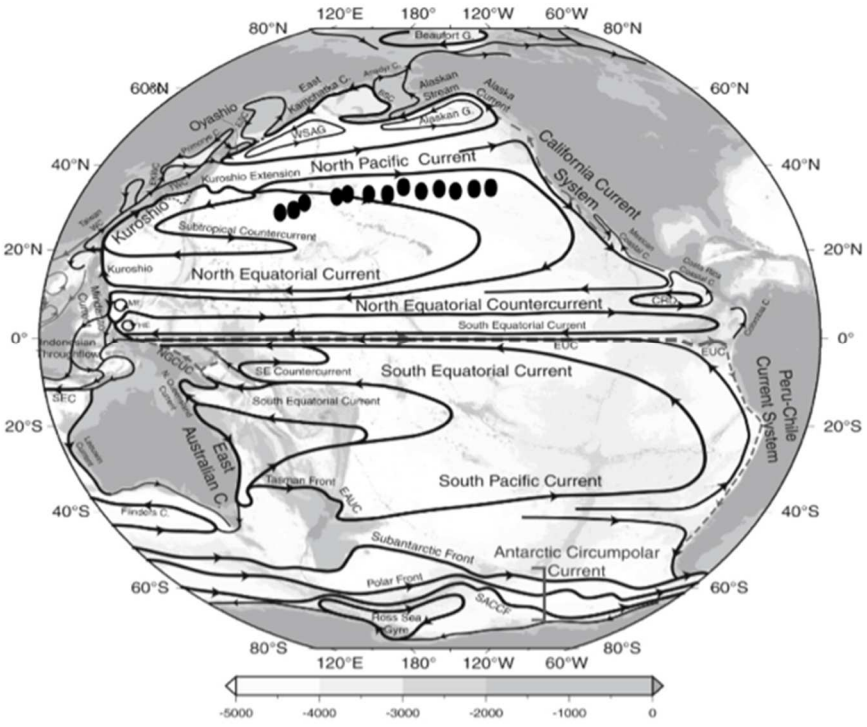

Figure 1: Surface circulation adapted from Talley et al (2011). Buoy deployment locations depicted as black dots.

The typical flow of the North Pacific Current during the winter involves an interaction between the Kuroshio and Oyashio currents. The winds and seas often intensify driven by the Arctic air that flows from northern Russia over the warm waters of the Kuroshio due to the East Asian Monsoon. Storms develop and high winds and seas are observed across the entire Pacific. Many of these storms flow Northeast and end in the Bering Sea or the Gulf of Alaska while others flow East across the Pacific zonally. In these winter storms, significant wave heights of 10m or higher are common. In the summer months, the North Pacific Current is quelled due to less intensified low pressure over Russia and smaller pressure gradients over the Kuroshio current. Figure 2 (Talley 2011) shows the mean wind stress and zonal wind stress for historical data from 1968-1996. Seasonality of the wind field is consistent with the wave field; stronger winds are observed in winter months.

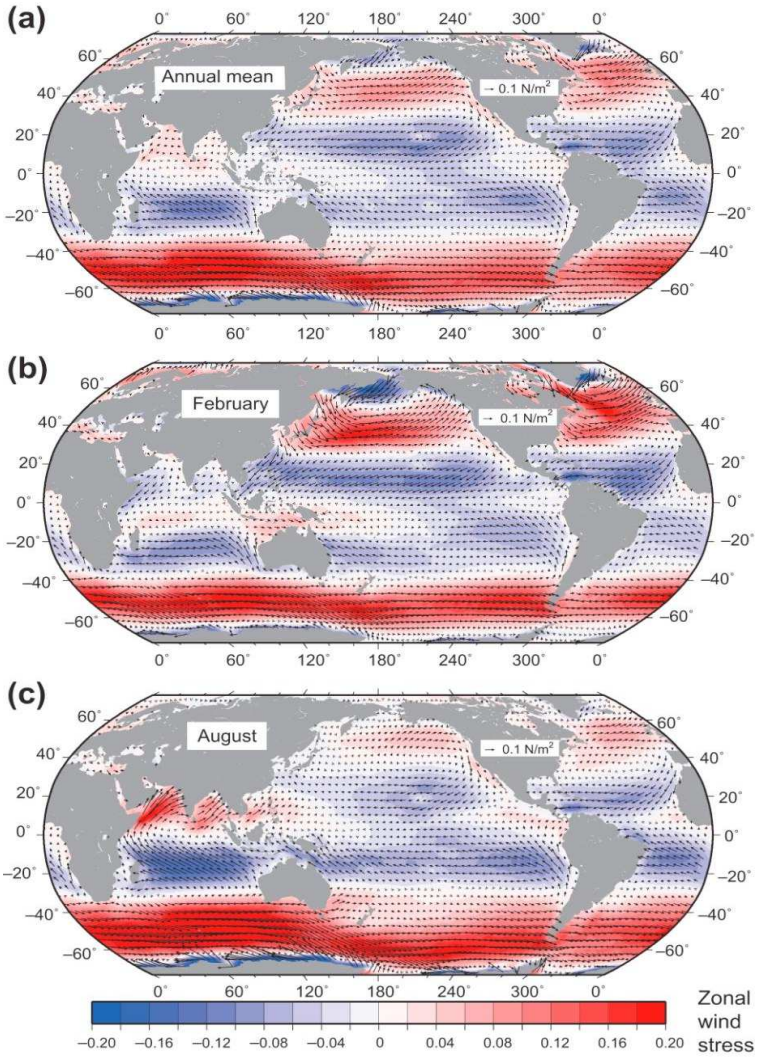

Figure 2: Adapted from Talley et al (2011) Mean wind stress (arrows) and zonal wind stress (color shading) (N/m2): (a) annual mean, (b) February, and (c) August, from the NCEP reanalysis 1968–1996 (Talley et al, 2011). The buoys in this study are predominately observed in a winter regime experiencing strong Westerlies.

This study utilizes a unique set of in-situ wave observations that align with the storm track of many extratropical storms in the Pacific Ocean. Thirteen large storms passed over the buoy array between December 2016 and June 2017. All storms originated off the coast of Japan with maximum significant wave height exceeding 12 meters. This thesis is organized into six sections. Section II describes the observations collected from drifting wave buoys. A statistical comparison of the bulk wave parameters

is presented in section III. Storm generation and arrival is discussed in section IV, followed by a wind-driven seas investigation in section V. The discussion and conclusion is section VI.

II. METHODS

The drifting wave buoys used in this study were developed at Scripps Institution of Oceanography by staff in the Coastal Observing Research and Development Center (CORDC), under the direction of Dr. Eric Terrill. The buoys used are 18 inches in diameter and communicate their data via Iridium, a commercial satellite constellation that provides the ability to transfer data globally. The buoys measure three-axis velocity using Doppler GPS for a fixed sample window and process the data onboard using standard Fourier techniques (Longuet-Higgins et al. 1963) to resolve the directional Fourier components. After every sampling period, data are relayed back to shore, and include the non-directional (1D) power spectrum, mean directions as a function of frequency, as well as the directional Fourier coefficients (a1, b1, a2, b2) (Otero 2012). Data undergo quality control processing and are stored in a netCDF data format for offline analysis.

Figure 3: Wave buoy deployed off the APL container ship in 2016. The buoys use alkaline batteries and are packaged in cardboard boxes to allow for ease of shipping and deployment.

As part of an Office of Naval Research Project to measure ocean wave conditions on the high seas, thirteen buoys were deployed zonally across the Pacific in the mid-latitudes on a single transit of an American Presidents Line (APL) (Figure 3) container ship. The vessel transit took place from the end of November 2016 to the beginning of

December 2016. At the close of the data collection, NRL provided a WW3 reanalysis that included modeled wave spectra at the time and position of each buoy. Unique to this inter-comparison study is the density and persistence of the observations in the Northern Pacific.

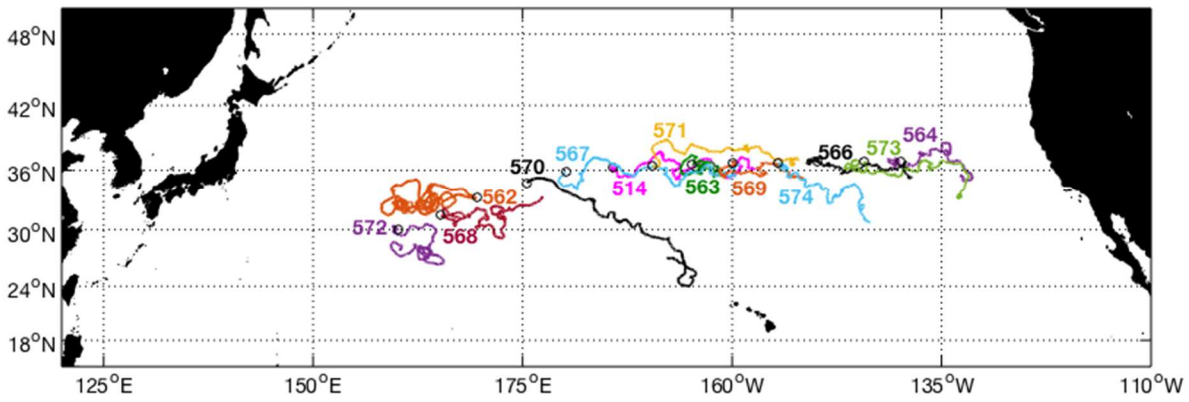

Figure 4: The tracks of the buoys during the six months of this study. The buoys followed the climatological pattern of the surface currents flowing west to east.

Figure 4 shows the tracks of all the buoys over the six months of this study. The distances and paths the buoys traveled varied between positions. Buoy 567, for example, traveled 4,550 km with a mean speed over ground of 0.72 m/s for a total distance of 1,853 km from its original starting position. Buoy 562, on the other hand, traveled 7,944.5 km with a mean speed over ground of 0.84 m/s but at the end of this study was only 13 km away from its original position. Figure 5a-b shows the initial position and the final position (respectively) of the buoys six months after their deployment.

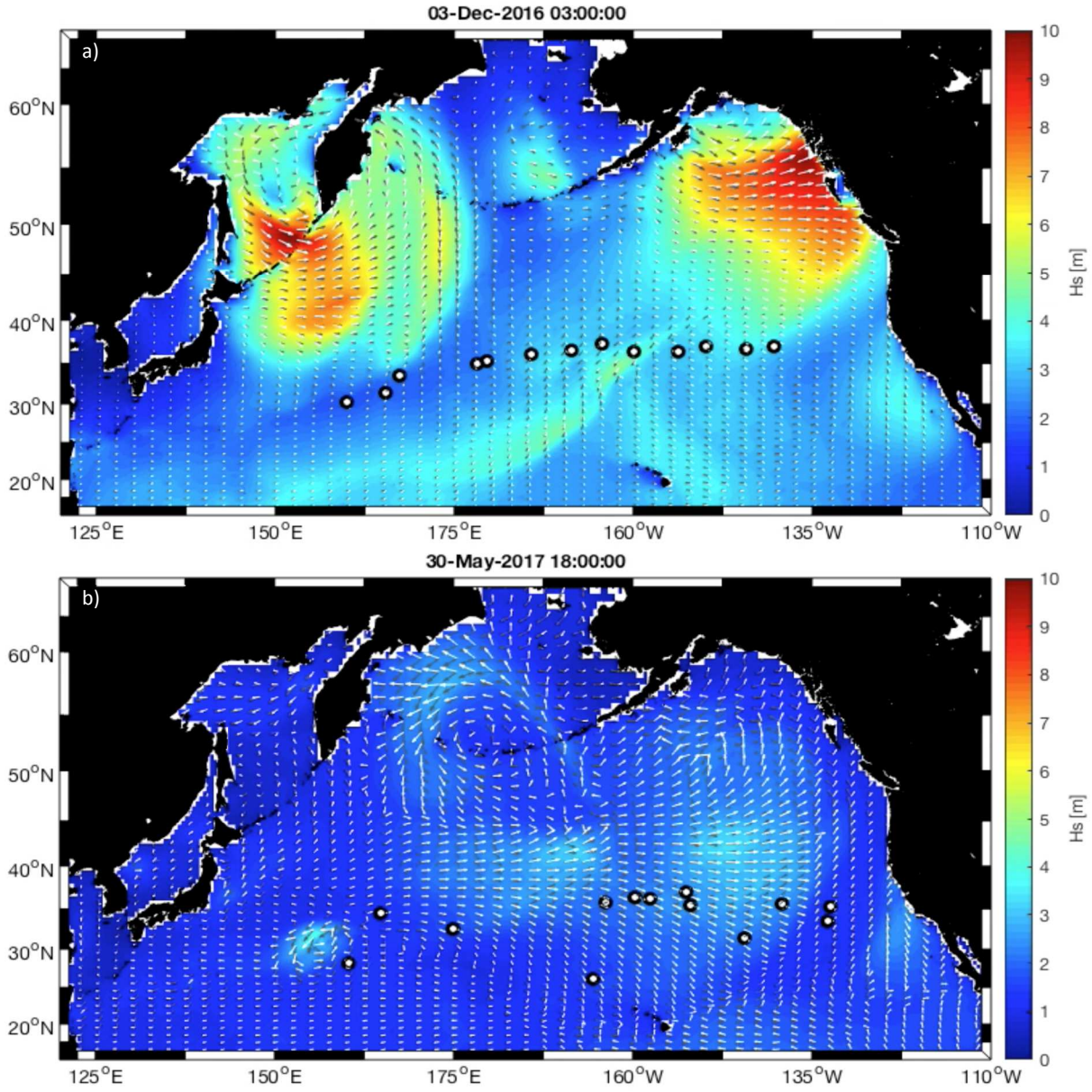

Figure 5: The a) initial position of the buoys as deployed by the APL container ship and b) position of the buoys as of 30 May 2017 (6 months after their deployment). The colors represent the significant wave height while the vectors represent the wind and wave direction. The Pacific basin has a strong seasonality in wave climate with larger wave heights in winter (a) relative to summer months (Fig b).

III. BULK WAVE PARAMETERS

The bulk wave parameters: significant wave height (H_s), peak period (T_p), peak direction (D_p), are computed from the omnidirectional energy spectrum. H_s is computed as four times the square root of the 0-th moment (m_0) over the frequencies 0.0576-0.726Hz. For further comparison, the average period (T_{avg}) and mean direction (D_m) at peak frequency are computed from the spectral output in an identical manner for the wave buoy and model output. The mean direction is derived from the Fourier coefficients following Kuik et al. 1988. Expressions for the parameters described above are:

$$m_0 = \int E(f)df \quad \text{(Equation 2)}$$

$$m_2 = \int f^2 E(f)df \quad \text{(Equation 3)}$$

$$T_{avg} = \sqrt{\left(\frac{m_0}{m_2}\right)} \quad \text{(Equation 4)}$$

$$b_1 = \int E(f)\sin(\theta)\, df \quad \text{(Equation 5)}$$

$$a_1 = \int E(f)\cos(\theta)\, df \quad \text{(Equation 6)}$$

$$D_m = \tan^{-1}\frac{b_1}{a_1} \quad \text{(Equation 7)}$$

where E(f) is the wave spectral density, f is the frequency and θ is the direction.

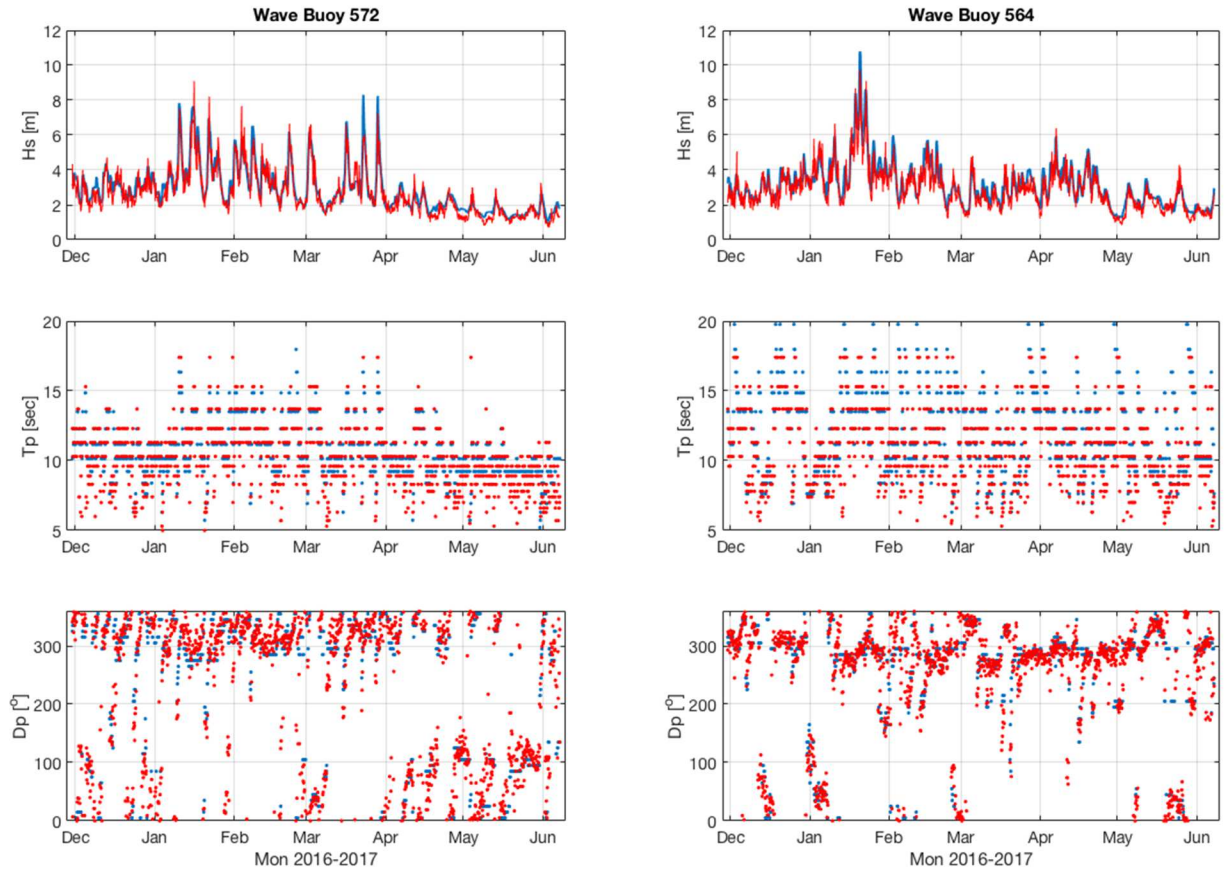

Figure 6: The bulk wave parameters: significant wave height (Hs), peak period (Tp), peak direction (Dp), are computed from the omnidirectional spectrum for buoys 572 and 564. While there is good agreement between WW3 (blue) and buoy measurements (red), large discrepancies exist during big events (Hs > 4m).

The bulk wave parameters, Hs, Tp, and Dp, are computed for buoys 572 and 564 (Figure 6). Overall general good agreement exists between the WW3 data and the buoy data for the entirety of the data series. Buoys 572 and 564 are used to show seasonal and spatial variability between the western (572) and eastern (564) Pacific. In the western Pacific, the winter months are seasonally characterized by larger significant wave height in comparison to other seasons. This is attributed to the proximity of the buoy to the storm generation off the east coast of Japan. Consequently, the peak period for this buoy is

often in the swell band in the winter when large storms are generated. Additionally, the peak direction of the buoy energy comes from the north to north west due to the generation and passing of storms. The eastern Pacific is characterized by less variance in significant wave heights and peak periods more often in the swell band as swells are known to cross the Pacific from west to east. Both buoys have predominant peak directions from the northwest with occasional nonlocal swell events from the Southern Ocean.

Table 1. Statistics for each buoy. Maximum cross correlation and root mean square error for Hs and Tp were calculated for each buoy. Buoys are organized based on start position location from West to East to show spatial variability. For the mean and maximum Hs, values in parentheses are for WW3.

Buoy SN	Initial position	Final position	Total Distance (km)	Distance traveled (km)	Mean Hs (m)	Max Hs (m)	Cc Hs (m)	RMSE Hs (m)	Cc Tp (s)	RMSE Tp (s)
572	30.02 N 160.33 E	28.12 N 160.52 E	4,739	245	2.71 (2.89)	9.10 (8.30)	0.938	0.47 m	0.49	1.62
568	31.40 N 165.31 E	32.47 N 175.53 E	4,866	1,154	3.00 (3.20)	11.64 (10.10)	0.930	0.57 m	0.55	1.87
562	33.22 N 168.99 E	34.46 N 165.27 E	7,945	13	3.27 (3.38)	12.86 (13.52)	0.928	0.60 m	0.57	1.67
570	35.21 N 176.96 E	26.46 N 165.83 W	4,664	1,812	2.947 (3.19)	9.09 (9.68)	0.916	0.54 m	0.53	2.04
567	35.56 N 179.87 E	36.42 N 159.59 W	4,550	1,853	3.44 (3.62)	10.06 (11.13)	0.938	0.45 m	0.45	2.00
514	36.13 N 174.22 W	36.21 N 157.56 W	4,277	1,529	3.38 (3.62)	9.52 (10.13)	0.932	0.61 m	0.66	1.91
571	36.37 N 168.89 E	37.08 N 152.44 W	3,948	1,545	3.27 (3.50)	9.85 (9.67)	0.911	0.62 m	0.60	2.23
563	37.25 N 164.38 W	35.84 N 163.75 W	3,603	152	3.29 (3.52)	10.71 (9.21)	0.917	0.61 m	0.68	1.95
569	36.37 N 159.67 W	35.30 N 151.72 W	3,353	813	3.22 (3.44)	9.43 (8.16)	0.910	0.59 m	0.58	2.26
574	36.31 N 153.69 W	31.28 N 134.24 W	3,484	1,213	2.95 (3.22)	9.37 (9.66)	0.922	0.57 m	0.49	2.62
566	36.99 N 149.77 W	35.46 N 138.99 W	3,278	1,022	3.05 (3.29)	8.85 (8.54)	0.925	0.57 m	0.52	2.63
573	36.77 N 144.15 W	33.47 N 132.67 W	3,907	1,089	2.97 (3.20)	8.87 (9.0)	0.922	0.53 m	0.47	2.83
564	36.90 N 140.08 W	35.17 N 132.40 W	3,238	686	2.91 (3.13)	9.72 (10.80)	0.922	0.53 m	0.55	2.85

Two error statistics are used as metrics for the model-data comparison, a correlation coefficient and a root mean squared error (RMSE). These statistics are listed for Hs and Tp for each buoy in Table 1 along with the distance traveled, mean and maximum Hs, and initial and final position of the buoys. A comparison of all model-buoy data for Hs and T_{avg} show that they are well correlated (0.92 and 0.89 respectively) with RMSEs of 0.57m and 0.63 seconds (Fig 7 a-b). RMSE of Hs>5m increases to 1.07m, nearly double that of the entire data set. Mean direction at the peak frequency shows good agreement other than a subset of the data that correspond to the largest model-data differences in peak period (Fig 7c). These data represent times when the peak period in WW3 is longer than in the buoy data and is often referred to as a "peak-picking" bias. This discrepancy is attributed to WW3 overestimating swell-band energy relative to the buoy data.

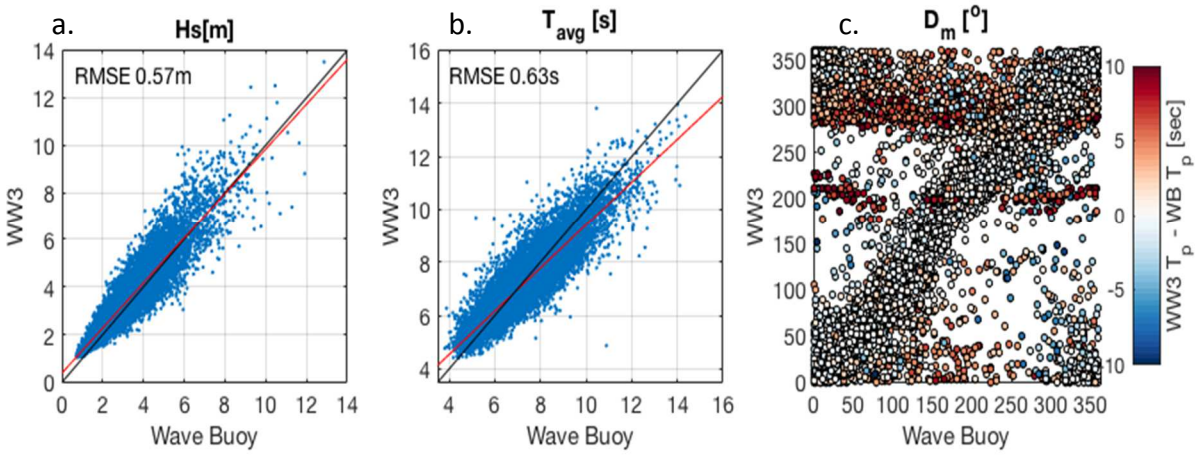

Figure 7: (a) and (b) Comparison of Hs, T_{avg} for all buoy data with computed correlation coefficients of 0.92 and 0.89, respectively. Black lines indicate a 1:1 fit while red lines are a linear regression. (c) Mean direction at peak frequency shows 'peak picking' bias for WaveWatch III.

Due to the swell-band bias, the wave spectra are partitioned to study swell and seas differences between the model and buoy data. Partitioning was done using a fixed cutoff at 0.125 Hz such that the swell band was between 0.05 Hz to 0.125 Hz and the seas band was between 0.125 and .073Hz. This corresponds to between 8-20 seconds for the swell, and 1.37-8 second period waves for the seas, respectively. Other cut off frequencies were investigated, but 0.125 Hz was chosen to try to best isolate the high frequency energy from the low frequency energy. Figure 8 shows the comparison between the Hs swell and seas bands for all buoys. Consistent with Rogers (2005), Figure 8 (right), shows a bias in WW3 in the seas band, indicating that the bias is not simply a coastal effect, but a pervasive feature of global wave models operating across ocean basins. In addition to the bias in the seas band in WW3, Fig. 8 (left) shows the spread increases when Hs is greater than 4m. The spread is disconcerting for the operational wave forecaster as extreme wave events forecasting is a critical need for operational planning and development of safety performance surfaces. For the U.S. Navy, being able to accurately forecast significant wave heights greater than 4m is exceptionally important for deck operations and navigation safety.

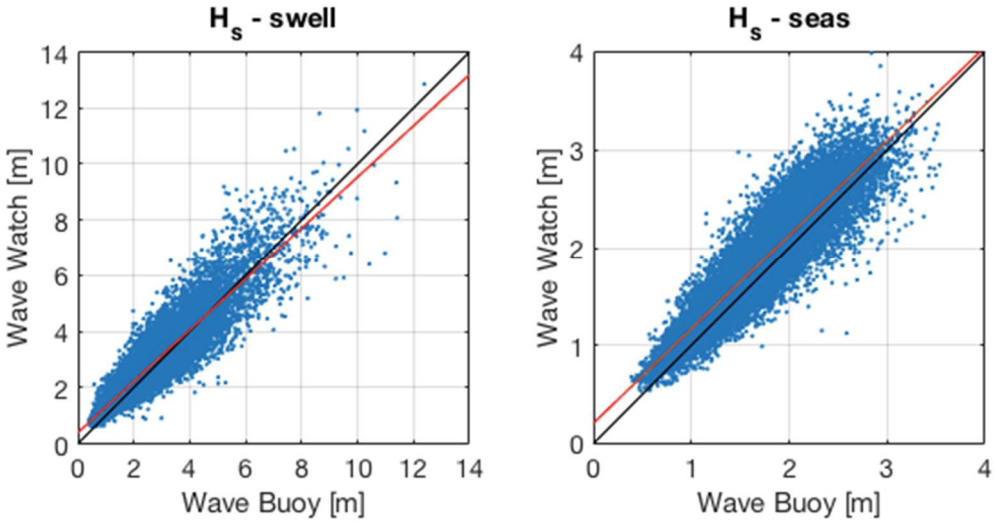

Figure 8: Comparison of WW3 Hs to the buoy Hs in the swell band (left) and seas band (right). Black lines indicate a 1:1 fit while red lines are a linear regression.

IV. STORM GENERATION AND ARRIVAL

A particular challenge for wave models is to accurately model the generation and propagation of storm systems. The timing and intensity of these systems determines the local wave conditions as well as the nonlocal properties of swell energy that propagate long distances. Here we study the propagation of storms across the Pacific by comparing data from systems that passed over multiple buoys in the array. We focus on three storm systems in January 2017 (Figure 9) generated off Japan that passed over multiple buoys as they moved eastward.

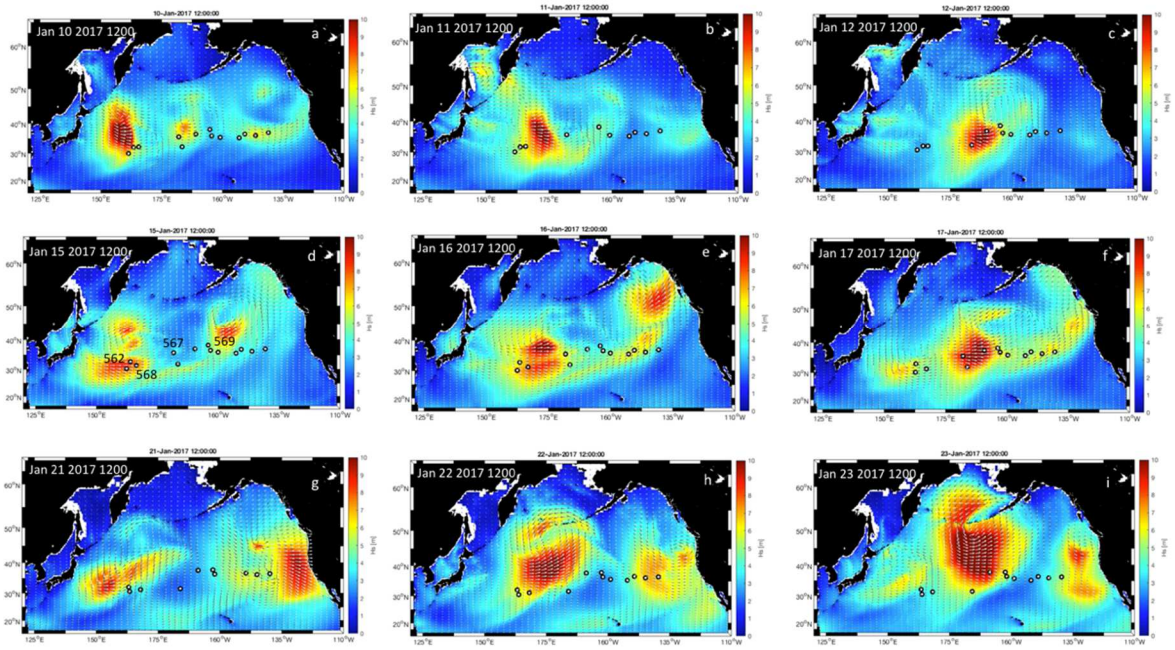

Figure 9: Three storm systems (a-c, d-f, g-i) generated off Japan that propagated eastward across the Pacific. Data from 4 buoys (562, 568, 567, 569), shown in d capture the evolution of the wave conditions associated with the systems.

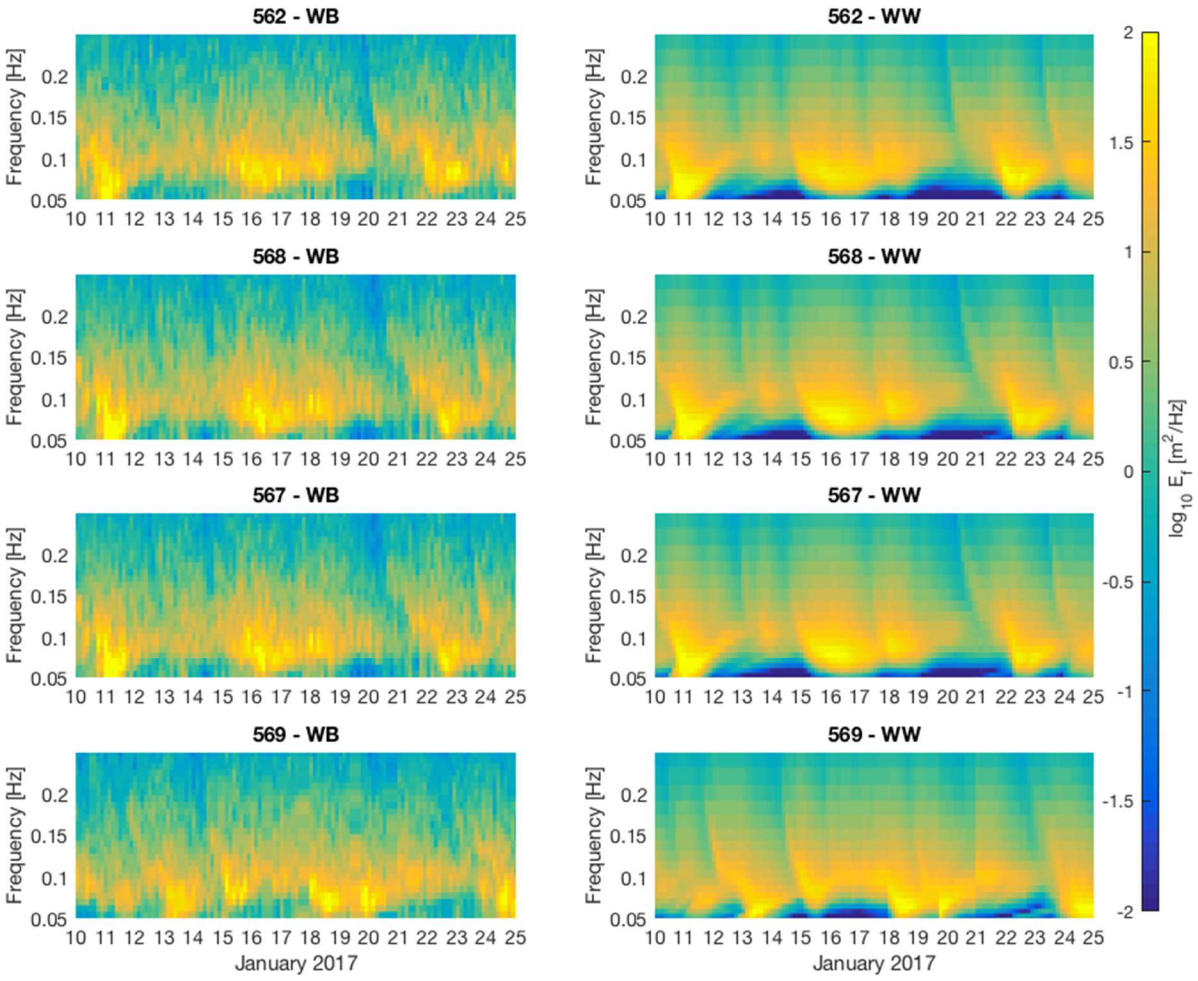

Figure 10: Spectrograms from the wave buoys and WW3 model output from the 4 buoys during the three storms shown in Figure 9.

In Figure 10, one can see the propagation of energy both temporally and spatially. The spectra show energy between 0.05 Hz and 0.25 Hz, 20 to 4 second period waves respectively. The WW3 spectra are very smooth and do not show all of the variability captured in the buoy observational spectra.

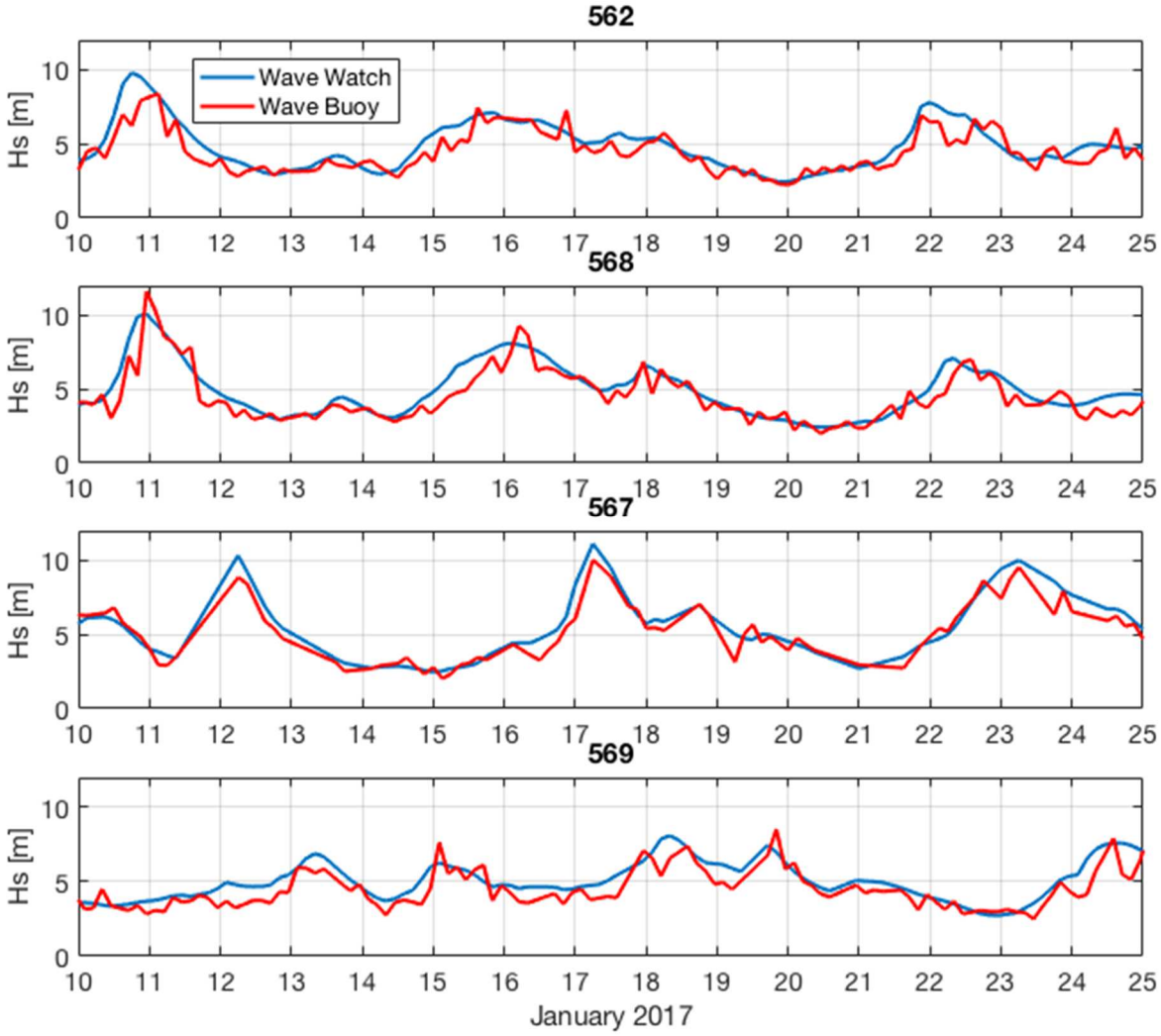

Figure 11: The Hs data comparison between the Buoy (blue) and the WW3 data (red) for the buoys shown in Figures 9-10.

Figure 11 displays the difference in the bulk parameter Hs over the three storms. During the period when the storm goes directly over the buoy field (for buoy 562 and 568) there is a difference between the prediction of WW3 and the observation from the buoy. A three-meter difference can be observed between the model and the buoy on January 10 for buoy 562 and buoy 568. Additionally, a timing error can be seen in the data. The model representation of the storm event fails to predict some of the variability in the

significant wave height during the storm. There is better agreement between the model prediction and buoy measurement of significant wave height when values are 4m or less. The storm path was directly over buoys 562 and 568 and outer bands passed over 567 and 569.

There are notable differences between the WW3 prediction and the buoy observation during the storms. The WW3 prediction of an event is often early and underestimates the observed significant wave height as the event progresses. WW3 shows the significant wave height increase occurring about 6-12 hours prior to the actual observation of the increase. To quantify the arrival bias, we compute the energy flux defined as:

$$Energy\ Flux = \rho g \int C_g(f) E(f) df \qquad \text{Equation (9)}$$

where ρ is the density of seawater, g is gravity, C_g(f)=g/(4πf) is the group speed for deep water waves, and f is the frequency. Figure 12 shows the model and buoy energy flux, computed between $0.8f_p$-$1.15f_p$, where f_p is the peak frequency of WW3. The energy flux predicted by the model precedes the energy flux of the buoy by, at times, six to ten hours. Additionally, the energy flux of the model tends to under-predict the energy flux associated with the buoy. We postulate this may be due to the wind field forcing and the timing associated with model's predicted arrival of the storm. The arrival time difference is operationally significant when time to destination and distance traveled are important factors in navigation.

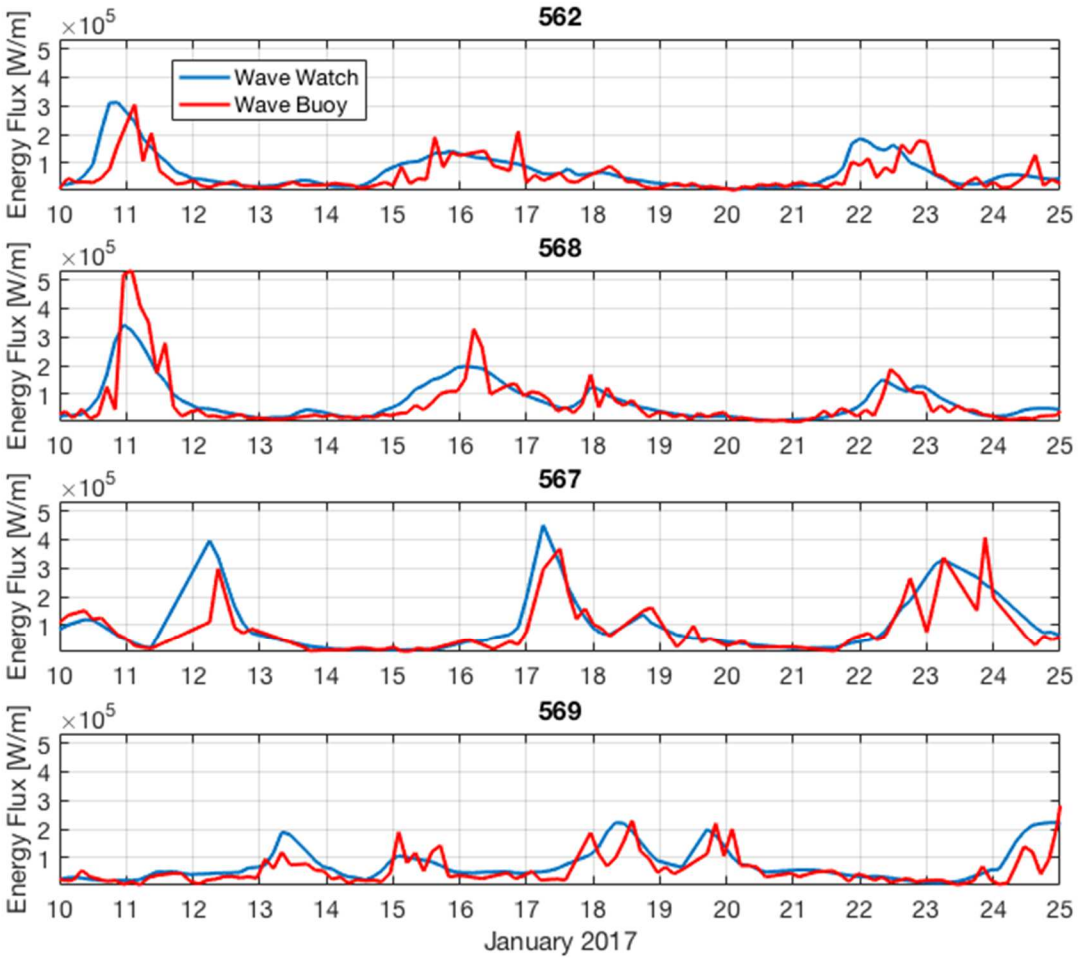

Figure 12: Energy flux comparison for a set of buoys (red) and WW3 (blue) as energy propagates across the Pacific during three January storm events. The buoys were west to east (top to bottom) respectively.

V. WIND-DRIVEN SEAS

Previous model-buoy comparison studies implicated the wind-field forcing as a source of error. To test whether the model wind-field product forced the ocean with accurate timing and strength, we compare significant wave height partitioned in the seas band. The discrepancy between model and data Hs seas is found to be wind speed dependent for wind speeds greater than 12m/s (Fig. 13). To further examine this dependence, the inverse wave age is estimated as:

$$(U_{10})/c_p \qquad \text{(Equation 10)}$$

Where c_p is the phase speed for deep water gravity waves ($c_p = gT_p/2\pi$) and U_{10} is the 10-m wind speed. The swell-driven regime occurs when the inverse wave age is <1 and young growing seas are indicated when the inverse wave age is > 1. Figure 13 shows greater bias in Hs in WW3 when wind speeds are high as well as when the wave regime is developing (Hanley et al. 2010). This indicates that there is an over prediction of WW3 in the seas band when seas are young and developing and that bias increases as wind speed increases. Further work is needed to determine whether this is due to errors in the wind field or to inaccurate parameterizations of energy input to the wave field at high wind speeds. No relationship between the seas bias and the co-alignment of the wind and waves was found (Fig 14).

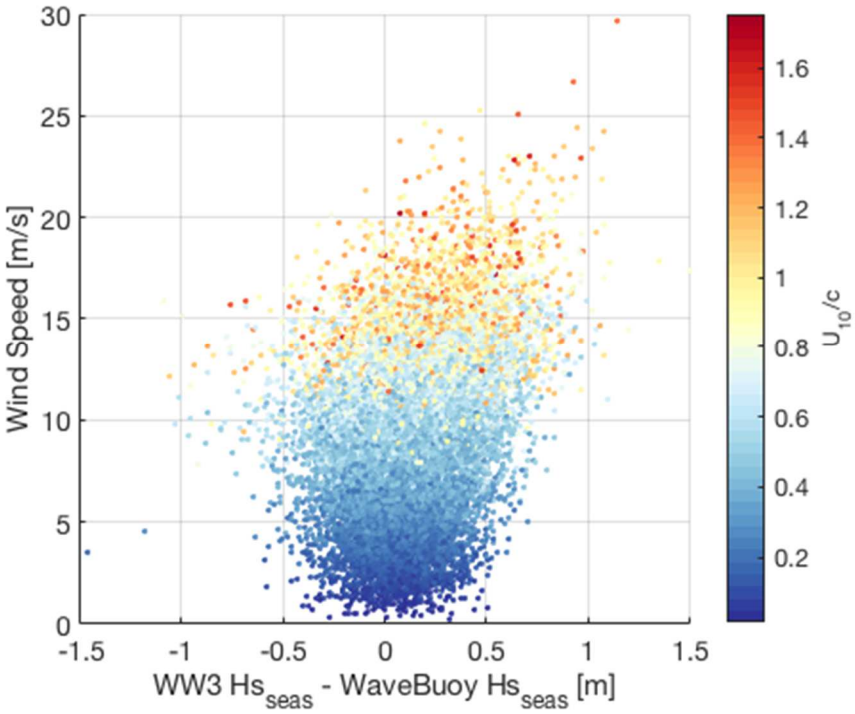

Figure 13: Difference between the WW3 Hs Seas and the Buoy Hs Seas as compared to wind speed. The Mean (WW3 Hs Seas-Buoy Hs Seas) = 0.1398 m. The bias in WW3 Hs seas increases with wind speed and inverse wave age (U10/cp) with > 1 indicating young and growing seas and indicating <1 older seas.

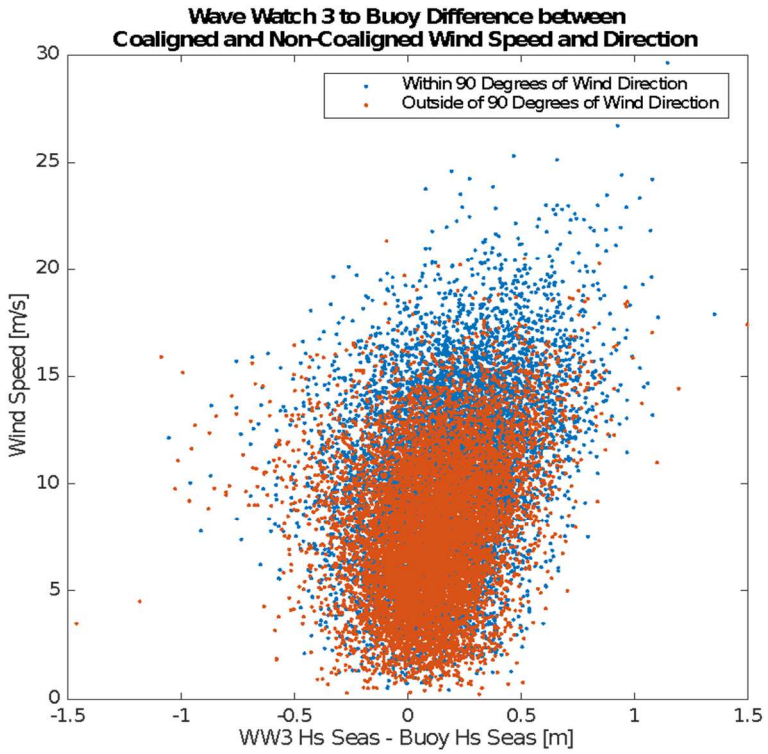

Figure 14: WW3 Hs seas to Buoy Hs seas within 90 degrees of wind direction to mean wind direction difference in blue compared to WW3 Hs seas to Buoy Hs seas with greater than 90 degrees of wind direction to mean wind direction difference (orange) as a function of wind speed.

Wave buoy and WaveWatch III data were compared for buoy 568 from 10 January 2017 to 25 Jan 2017 to study the role of the wind field in the arrival time and Hs seas biases. Figure 15 a., b. shows the wave buoy (568) and WW3 (respectively) mean wave direction as a function of frequency and time. The wind and wave direction have good agreement during this period (Fig. 15 a, b, c). Figure 15 d. compares the wave buoy Hs seas (red) to the WW3 Hs seas (blue) and the WW3 wind speed (black). During the first two storms (Jan 10-12 and 15-17), increases in WW3 Hs seas lead buoy observations by 6-10 hours. The early increase in Hs seas corresponds to an increase in the wind speed suggesting that the disparity in Hs seas is due to errors in the NAVGEM wind field.

Additionally, the magnitude of Hs seas in the buoy observations is consistently lower than WW3 during the storm events suggesting that either the model wind is too strong or that energy input to the wave field during high winds is parameterized improperly.

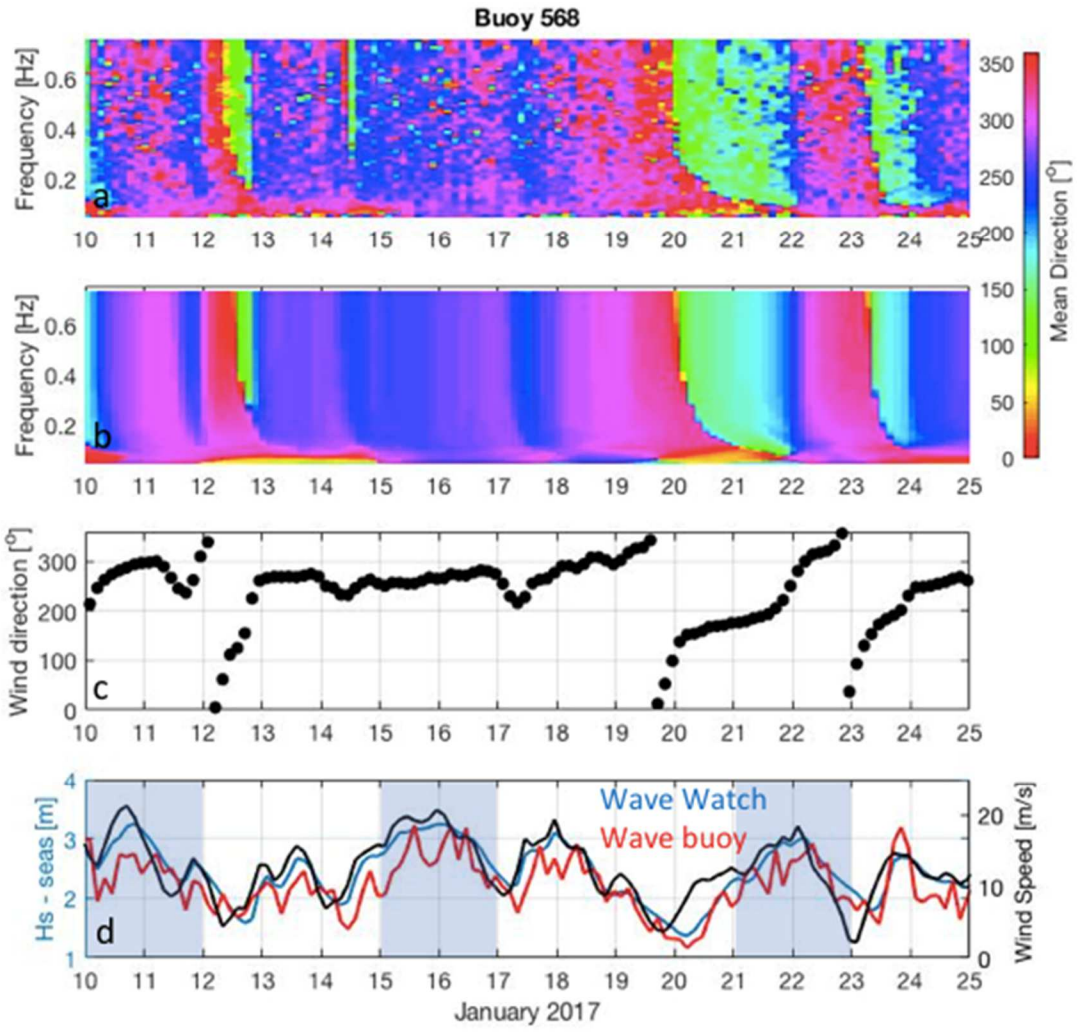

Figure 15: a) Buoy 568 mean direction b) WW3 568 mean direction c) model wind forcing direction and d) Hs seas for buoy (blue) and WW3 (red) and wind speed in black. In (d), the wind speed and WW3 Hs seas tend to increase before the increase in Hs seas for the buoy (red).

VI. DISCUSSION AND CONCLUSION

This thesis reports on the results from a novel comparison of the open ocean model WaveWatch III to thirteen drifting, GPS-based wave buoys during which bulk and spectral data were acquired over a wide zonal range of the northern Pacific. The inexpensive buoy technology developed at Scripps provides a new platform for conducting array-based, persistent observation of the ocean to examine basin-scale model performance normally not feasible without great expense. The data from this array deployment provides insight into the open ocean prediction capability for WaveWatch III. Overall, good agreement was found between the WW3 output and the buoy data for the entirety of the data series, especially for bulk properties Hs and T_{avg} that show a correlation of 0.92 and 0.89 respectively, and RMSEs of 0.57m and 0.63 seconds but RMSE nearly doubles to 1.07m when Hs>5m. In general, the mean direction of modeled waves has good agreement with the observations, except during times when errors in modeled peak period are high. During these times, the model was biased toward the swell energy, and overestimated the swell band energy as well as Hs relative to the buoy data. Additionally, when the significant wave height was greater than four meters, an increased spread was noted between model and buoy data, a concern for the forecaster dependent on the accuracy of extreme event prediction.

Model performance was assessed for storm arrival times as the buoys were well aligned with the track of many storm systems generated off Japan. An investigation of both the wave spectra and energy flux of the waves illustrate disparities between the model and observed data. In particular, the wave spectra from the model are smoother

in comparison to the observations which reflect wind variability and atmospheric turbulence not represented in the large-scale wind forcing. The energy fluxes predicted by the model are found to arrive earlier than those observed by the buoys during storm events. Furthermore, the modeled energy fluxes are generally lower than observed. These arrival errors can lead to significant wave height differences in excess of three meters during storms. This is meaningful in that over or under prediction of this magnitude could be detrimental to the safe navigation of U.S. Navy vessels which avoid significant wave heights in this range. Additionally, a timing error of 6-10 hours was noted during storm propagation across the Pacific basin. The errors in this timing could adversely affect the safety of navigation as well as the time cargo ships take to deliver their cargo. It should be emphasized that these biases and errors are found only during the storm events, and that the model is found to resolve the observational environment well when the significant wave height is less than four meters, and during times of non-event winds.

Finally, WW3 over predicted significant wave height in the seas band during model wind speeds greater than approximately 12 m/s. During storm events the model wind and Hs seas were early relative to the buoy Hs seas suggesting the arrival bias is due to errors in the NAVGEM wind product. Further work is needed to determine whether Hs seas biases during high winds are due to errors in the NAVGEM wind field or in the model parameterization of wind energy to the wave field.

As in previous studies, model-data biases in this study are postulated to be associated with errors in the wind-forcing field. Due to the austere location of these buoys, assimilation of real-time wind data is not available. As the U.S. Navy continually operates

in these locations, tuning the model to account for the bias in the wind field would allow greater accuracy in the forecast. As this was a hindcast study, the comparison was made between observed data and modeled 'nowcast' data. Therefore, there may be greater discrepancy in the forecast of the model compared to the actual conditions. One approach to improving forecasts would be for ocean basin wave models to assimilate in-situ wave data from arrays of drifters, such as the ones used in this study. Further studies will be required to develop these procedures. Honing the forecast will provide situational awareness for the warfighter, improved safety for at-sea operations, as well as potentially increase profits associated with optimal routing of commercial cargo ships.

LIST OF REFERENCES

1. Ardhuin, F., Rogers, E., Babanin, A. V., Filipot, J. F., Magne, R., Roland, A., ... & Collard, F. (2010). Semiempirical dissipation source functions for ocean waves. Part I: Definition, calibration, and validation. *Journal of Physical Oceanography*, *40*(9), 1917-1941.

2. Bidlot, J. R., Holmes, D. J., Wittmann, P. A., Lalbeharry, R., & Chen, H. S. (2002). Intercomparison of the performance of operational ocean wave forecasting systems with buoy data. *Weather and Forecasting*, *17*(2), 287-310.

3. Hanley, K. E., Belcher, S. E., & Sullivan, P. P. (2010). A global climatology of wind–wave interaction. *Journal of Physical Oceanography*, *40*(6), 1263-1282.

4. Kuik, A. J., Van Vledder, G. P., & Holthuijsen, L. H. (1988). A method for the routine analysis of pitch-and-roll buoy wave data. *Journal of physical oceanography*, *18*(7), 1020-1034.

5. Longuet-Higgins, M. S., D. Cartwright, and N. Smith, 1963: Observations of the directional spectrum of sea waves using the motions of a floating buoy. *Ocean Wave Spectra: Proceedings of a Conference*, Prentice-Hall, 111–136.

6. McNally, G. J., Patzert, W. C., Kirwan, A. D., & Vastano, A. C. (1983). The near-surface circulation of the North Pacific using satellite tracked drifting buoys. *Journal of Geophysical Research: Oceans*, *88*(C12), 7507-7518.

7. Otero, Mark., Wave Buoy Spectral Processing. 06 December 2012 for Coastal Observation Research and Development Center, Marine Physical Laboratory, Scripps Institution of Oceanography.

8. Rogers, W. E., Wittmann, P. A., Wang, D. W., Clancy, R. M., & Hsu, Y. L. (2005). Evaluations of global wave prediction at the Fleet Numerical Meteorology and Oceanography Center. *Weather and forecasting*, *20*(5), 745-760.

9. Smith, C. B. (2007, September). Extreme waves and ship design. In *10th International Symposium on Practical Design of Ships and Other Floating Structures, Houston, USA*.

10. Talley, L. D., Pickard, G, Emery, W.J. & Swift, J.H., 2011. Descriptive Physical Oceanography: An Introduction. Academic Press, p.308.

11. Tolman, H. L., & Chalikov, D. (1996). Source terms in a third-generation wind wave model. *Journal of Physical Oceanography*, *26*(11), 2497-2518.

12. Tolman, H. L., Balasubramaniyan, B., Burroughs, L. D., Chalikov, D. V., Chao, Y. Y., Chen, H. S., & Gerald, V. M. (2002). Development and implementation of wind-generated ocean surface wave Modelsat NCEP. *Weather and Forecasting*, *17*(2), 311-333.

13. Wingeart, K. M., Herbers, T. H., O'Reilly, W. C., Wittmann, P. A., Jensen, R. E., & Tolman, H. L. (2002). Validation of operational global wave prediction models with spectral buoy data. In *Ocean Wave Measurement and Analysis (2001)* (pp. 590-599).